Magn Reson Med Sci
doi:10.2463/mrms.mp.2023-0115

Published Online: May 22, 2024

MAJOR PAPER

Thin-slice 2D MR Imaging of the Shoulder Joint Using Denoising Deep Learning Reconstruction Provides Higher Image Quality Than 3D MR Imaging

Takahide Kakigi[1*], Ryo Sakamoto[1,2], Ryuzo Arai[3], Akira Yamamoto[1,4], Shinichi Kuriyama[5], Yuichiro Sano[6], Rimika Imai[6], Hitomi Numamoto[7,8], Kanae Kawai Miyake[1,8], Tsuneo Saga[1,8], Shuichi Matsuda[5], and Yuji Nakamoto[1]

Purpose: This study was conducted to evaluate whether thin-slice 2D fat-saturated proton density-weighted images of the shoulder joint in three imaging planes combined with parallel imaging, partial Fourier technique, and denoising approach with deep learning-based reconstruction (dDLR) are more useful than 3D fat-saturated proton density multi-planar voxel images.

Methods: Eighteen patients who underwent MRI of the shoulder joint at 3T were enrolled. The denoising effect of dDLR in 2D was evaluated using coefficient of variation (CV). Qualitative evaluation of anatomical structures, noise, and artifacts in 2D after dDLR and 3D was performed by two radiologists using a five-point Likert scale. All were analyzed statistically. Gwet's agreement coefficients were also calculated.

Results: The CV of 2D after dDLR was significantly lower than that before dDLR ($P < 0.05$). Both radiologists rated 2D higher than 3D for all anatomical structures and noise ($P < 0.05$), except for artifacts. Both Gwet's agreement coefficients of anatomical structures, noise, and artifacts in 2D and 3D produced nearly perfect agreement between the two radiologists. The evaluation of 2D tended to be more reproducible than 3D.

Conclusion: 2D with parallel imaging, partial Fourier technique, and dDLR was proved to be superior to 3D for depicting shoulder joint structures with lower noise.

Keywords: *deep learning, magnetic resonance imaging, shoulder, thin-slice, two-dimensional*

Introduction

MRI technology is advancing and is rapidly becoming indispensable for diagnosis and treatment. For musculoskeletal MRI as well, acceleration techniques such as parallel imaging, compressed sensing, and deep learning approaches are being used, leading to shorter acquisition times and to improvement of image quality.[1–5]

Conventionally, MRI of the shoulder joint has been based on scanning 2D images, but 3D images, which can be evaluated in thinner slices, have also been scanned to assess anatomical structures and lesions in greater detail.[6] Included in 3D imaging techniques are imaging sequences such as multi-planar voxel (MPV; Canon Medical Systems, Otawara, Japan) and sampling perfection with application optimized contrast using different flip angle evolutions (Siemens Healthineers, Erlangen, Germany) based on fast spin echo. These 3D methods collect magnetic resonance signals by volume excitation and obtain thinner slice thicknesses than 2D images; multi-planar reconstruction (MPR)

[1]Department of Diagnostic Imaging and Nuclear Medicine, Kyoto University Graduate School of Medicine, Kyoto, Kyoto, Japan
[2]Department of Real World Data Research and Development, Kyoto University Graduate School of Medicine, Kyoto, Kyoto, Japan
[3]Department of Orthopaedic Surgery, Kyoto Katsura Hospital, Kyoto, Kyoto, Japan
[4]Center for Medical Education, Kyoto University Graduate School of Medicine, Kyoto, Kyoto, Japan
[5]Department of Orthopaedic Surgery, Kyoto University Graduate School of Medicine, Kyoto, Kyoto, Japan
[6]MRI Systems Division, Canon Medical Systems Corporation, Otawara, Tochigi, Japan
[7]Division of Clinical Radiology Service, Kyoto University Hospital, Kyoto, Kyoto, Japan
[8]Department of Advanced Medical Imaging Research, Kyoto University Graduate School of Medicine, Kyoto, Kyoto, Japan
*Corresponding author: Department of Diagnostic Imaging and Nuclear Medicine, Kyoto University Graduate School of Medicine, 54 Shogoin Kawahara-cho, Sakyo-ku, Kyoto, Kyoto 606-8507, Japan. Phone: +81-75-751-3760, Fax: +81-75-771-9709, E-mail: tkakigi@kuhp.kyoto-u.ac.jp

Received: September 7, 2023 | Accepted: March 29, 2024

images are also possible.[4,6–9] In contrast, conventional 2D images present advantages of high tissue contrast and in-plane spatial resolution, but with the disadvantages of thick slices and partial volume effects.[6,10,11] To benefit completely from the advantages of thin-slice 2D images, low SNR and a longer scan time to obtain three orthogonal imaging planes must be overcome. One widely used acceleration technique is partial Fourier technique. This reconstruction technique creates an entire MRI using not all but only more than half of the data of the k-space. Partial Fourier technique can shorten the acquisition time by reducing k-space phase encoding, but it comes at the expense of SNR.[12,13] To increase SNR and to improve image quality, various techniques have been developed recently using deep learning approaches. Denoising techniques with deep learning reconstruction (dDLR) are reportedly useful in various areas of MRI application. The Advanced intelligent Clear-IQ Engine (AiCE; Canon Medical Systems) learns only noise patterns by deep learning. Moreover, it can adapt to the obtained image data. This technology enables the removal of noise only from low SNR images and enables increased SNR for image quality improvement.[4,5,14–24] Using this technique, high-resolution thin-slice 2D images with low noise can be achieved even when a rapid acquisition protocol using both parallel imaging and partial Fourier technique is applied. The 2D rapid acquisition will also enable multi-planar imaging (e.g., 2D imaging in three imaging planes) in a clinically acceptable scan time.

For this study, we examined whether thin-slice 2D fat-saturated proton density-weighted images (FS-PDWIs) of the shoulder joint in three imaging planes combined with parallel imaging, partial Fourier technique, and dDLR are more useful than 3D fat-saturated proton density multi-planar voxel (FS-PD MPV) images.

Materials and Methods

Study design

This institutional review board (Ethics committee of Kyoto University graduate school and faculty of medicine), approved as prospective study, was registered with the Japan Registry of Clinical trials (jRCT: s052200013). It was performed in accordance with the ethical standards as laid down in the 1964 Declaration of Helsinki and its later amendments. Written informed consent was obtained from all individual participants included in the study. The primary end points were evaluation of the denoising effects of dDLR on thin-slice 2D FS-PDWIs with both parallel imaging and partial Fourier technique by comparing the coefficient of variation (CV, standard deviation (SD) divided by mean) of the signal for thin-slice 2D FS-PDWIs before dDLR, thin-slice 2D FS-PDWIs after dDLR, and 3D FS-PD MPV images. The secondary end points were evaluation of the visualization of anatomical structures, image noise, and motion artifacts between dDLR-applied thin-slice 2D FS-PDWIs and 3D FS-PD MPV images.

Subjects

We recruited patients who were going to receive MRIs for shoulder problems between September 2020 and March 2021. Inclusion criteria were that they were at least 20 years of age and agreed to participate in our study. Exclusion criteria included general contraindications for MRI and prior shoulder surgery.

MR image acquisition

MR scans were conducted using a 3T scanner (Vantage Centurian; Canon Medical Systems) with a 16-channel flex coil. The patients were placed in a supine position with the shoulder and arm to the body in neutral position. In accordance with our institutional protocol for routine shoulder MRI, proton density-weighted images (TR ms/TE ms, 3610/22; 320×384 matrix; 3 mm thickness), T2-weighted images (TR ms/TE ms, 6726/100; matrix, 320×320; 3 mm thickness), and FS-PDWIs (TR ms/TE ms, 4083/50; matrix, 320×320; 3 mm thickness) were acquired in each of the three imaging planes (oblique coronal, axial, and oblique sagittal images). The oblique coronal imaging plane was prescribed from the axial image at the level of the supraspinatus central tendon parallel to the low signal intensity tendon. The oblique sagittal imaging plane was selected perpendicular to the oblique coronal imaging plane. Additionally for this study, we performed thin-slice 2D FS-PDWIs (0.62×0.5 mm resolution, 1 mm thickness) in three imaging planes (oblique coronal, axial, and oblique sagittal images) and oblique coronal 3D FS-PD MPV images (voxel dimensions, $0.7 \times 0.7 \times 0.7$ mm). Oblique sagittal and axial images were created from the oblique coronal 3D FS-PD MPV images (0.7 mm slice thickness, 0.7 mm slice spacing). The acquisition times for thin-slice 2D FS-PDWIs (oblique coronal, oblique sagittal, and axial images all together) and 3D FS-PD MPV images were 8 mins and 6 mins 32 sec, respectively (Table 1). Both parallel imaging and partial Fourier technique were used to reduce the acquisition time to scan three imaging planes of thin-slice 2D images. The 3D voxel dimension was determined after considering the acquisition time and image quality.

dDLR application to MRI data

dDLR as a product (AiCE) was adapted to thin-slice 2D FS-PDWIs in three imaging planes (oblique coronal, axial, and oblique sagittal images), as described in earlier reports.[4]

dDLR technique is based on the shrinkage convolutional neural network (SCNN), which can adjust the noise power of the input by using the CNN with soft-shrinkage activation functions. SCNN can accommodate various noise levels by setting the appropriate noise for each input image. SCNN performs noise reduction directly in the image domain. dDLR is based on SCNN, but dDLR differs from SCNN in that it performs noise reduction by learning the noise threshold of the high-frequency components extracted by a discrete cosine transform.[4,5,15,16,25]

Table 1 MR Pulse Sequence Protocol for thin-slice 2D FS-PDWIs and 3D FS-PD MPV images

Parameters	2D MRI protocol			3D MRI protocol
	thin-slice 2D FS-PDWIs			3D FS-PD MPV images
Orientation	Oblique coronal	Oblique sagittal	Axial	Oblique coronal
TR, ms	3363	4324	3363	900
TE, ms	50	50	50	48.8
Acceleration factor	2.5	2.5	2.5	2
Echo train length	7	7	7	44
Receiver bandwidth, Hz/pixel	195.3	195.3	195.3	488.2
Flip/flop angle, degree	90/150	90/150	90/150	90/170 (Variable)
FOV, mm	160 × 160	160 × 160	160 × 160	180 × 180
Matrix	256 × 320	256 × 320	256 × 320	256 × 256
Slice thickness/gap, mm	1/0	1/0	1/0	0.7/0
Voxel dimension, mm	0.625 × 0.5 × 1	0.625 × 0.5 × 1	0.625 × 0.5 × 1	0.7 × 0.7 × 0.7
Voxel volume, mm^3	0.313	0.313	0.313	0.343
Number of excitations	1	1	1	1
Number of slices	70	90	70	95
Concatenations	2	2	2	1
Phase encoding direction	Anterior to posterior	Anterior to posterior	Anterior to posterior	Right to left
Phase sampling, %	63.6	63.6	63.6	55
Acquisition time	2 min, 50s	3 min, 2s	2 min, 8s	6 min, 32s

FS-PDWIs, fat-saturated proton density-weighted images; FS-PD MPV, fat-saturated proton density multi-planar voxel.

Quantitative image evaluation methods

To evaluate the effects of adapting dDLR on the image noise on thin-slice 2D FS-PDWIs and to compare the image noise with 3D FS-PD MPV images, two board-certified radiologists with 18 years of experience (R.S. and T.K.) placed the ROIs separately on one representative slice of the metaphysis of the humerus, the supraspinatus muscle, and the superior portion of the labrum on a medical professional imaging viewer (EV Insite; PSP, Tokyo, Japan) and obtained the mean, SD, and CV (SD divided by mean) of the signal in oblique coronal thin-slice 2D FS-PDWIs before and after adaptation of dDLR and oblique coronal 3D FS-PD MPV images. Only one evaluation was performed. The ROI sizes were 40 mm^2, 20 mm^2, and 5 mm^2, respectively, for the metaphysis of the humerus, the supraspinatus muscle, and the superior portion of the labrum (Fig. 1).

Qualitative image evaluation methods

Corresponding thin-slice 2D FS-PDWI and 3D FS-PD MPV image datasets were separated and anonymized. All image datasets were reviewed in a randomized order. All radiographic reports and patient clinical information were blinded. Two board-certified radiologists (R.S. and T.K.) evaluated each study independently using a medical professional imaging viewer (EV Insite R; PSP). Before evaluation, the readers mutually discussed the evaluation method and agreed to proceed. Image evaluation was performed at approximately 1 lux using a 30-inch diagnostic-quality color liquid crystal display monitor that had been calibrated to Digital Imaging and Communications in Medicine standards (RadiForce RX660; EIZO, Ishikawa, Japan). All data were displayed in a 2 × 2 layout on the display monitor. Both readers were allowed to set the windows and levels as desired and were permitted to magnify and scroll freely.

Visualization of the anatomical structure, image noise, and motion artifacts were evaluated. All were evaluated on a five-point Likert scale.[7]

The following anatomical structures were selected for visual evaluation of the anatomical structure: (i) supraspinatus tendon (SSp), infraspinatus tendon, and subscapularis tendon; (ii) long head of biceps tendon (comprehensive evaluation on oblique coronal, oblique sagittal, and axial planes in thin-slice 2D FS-PDWIs and 3D FS-PD MPV images for (i) and (ii)); (iii) cartilage of glenohumeral joints; and (iv) labrum (comprehensive evaluation on oblique coronal and axial planes in thin-slice 2D FS-PDWIs and 3D FS-PD

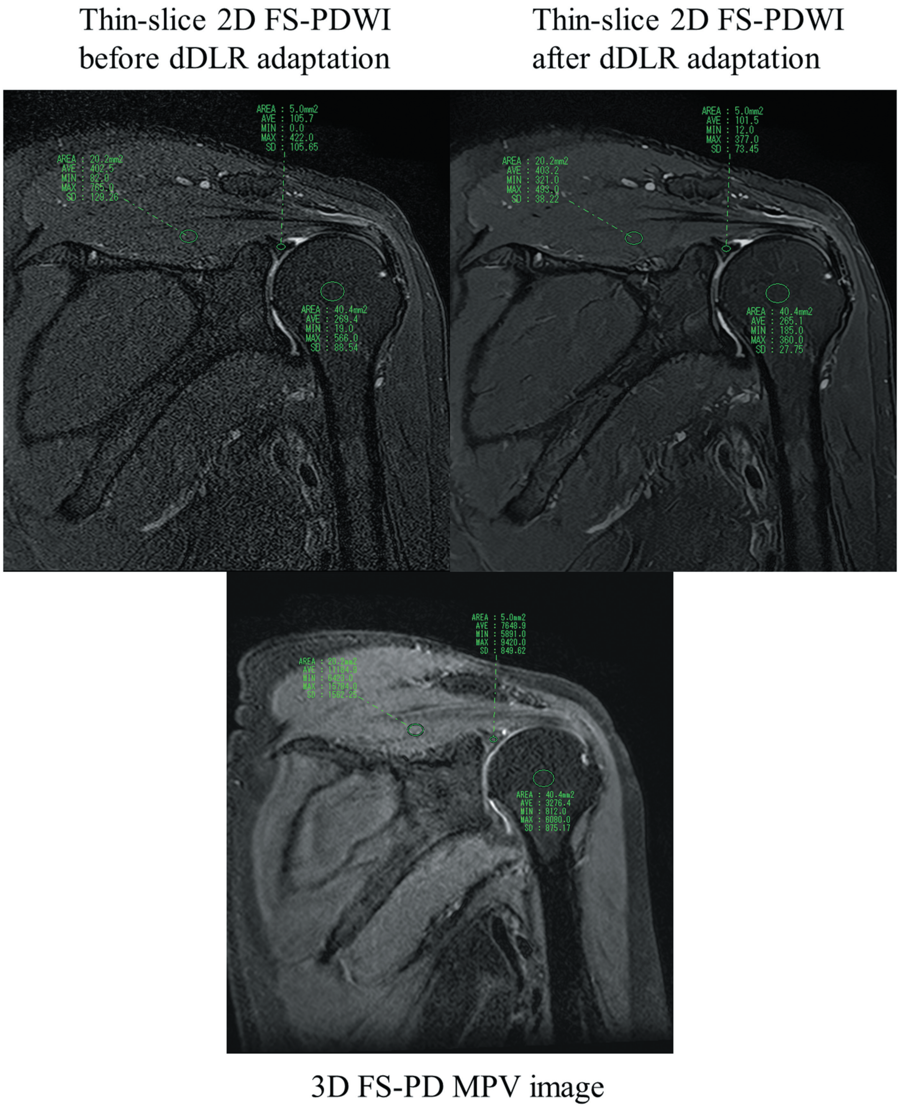

Fig. 1 Placement of ROIs. ROIs were placed at the metaphysis of the humerus, the supraspinatus muscle, and the superior portion of the labrum in oblique coronal thin-slice 2D FS-PDWI before and after adaptation of dDLR and the oblique coronal 3D FS-PD MPV image. 2D FS-PDWI, two-dimensional fat-saturated proton density-weighted image; dDLR, denoising approach with deep learning-based reconstruction; 3D FS-PD MPV, three-dimensional fat-saturated proton density multi-planar voxel.

MPV images for (iii) and (iv)). The internal structural visuality, contours, and contrasts were evaluated comprehensively. A five-point Likert scale was used to record the evaluation: 1 point, very poor; 2 points, bad; 3 points, sufficient; 4 points, good; 5 points, very good. When lesion was present on the target structure, visuality of normal structures was evaluated to the extent that normal anatomical structures could be recognized.

Image noise was evaluated comprehensively on oblique coronal, oblique sagittal, and axial planes in thin-slice 2D FS-PDWIs and 3D FS-PD MPV images. A five-point Likert scale was used to record the evaluation: 1 point, severe – difficult to assess for diagnosis; 2 points, moderate – remarkable noises are present; 3 points, mild – noises are seen, but not so readily apparent; 4 points, minimal – few noises are visible; 5 points, none.

Motion artifacts were evaluated by comprehensive assessment of the oblique coronal, oblique sagittal, and axial planes in thin-slice 2D FS-PDWIs and 3D FS-PD MPV images using a five-point Likert scale: 1 point, severe – difficult to assess for diagnosis; 2 points, moderate – remarkable artifacts are present; 3 points, mild – artifacts are seen, but not so readily apparent; 4 points, minimal – few artifacts are visible; 5 points, none.

Statistical analysis

Statistical analyses were performed using software (JMP Pro 15.2.0; SAS Institute, Cary, NC, USA). For quantitative evaluation, intraclass correlation coefficients (ICCs) of CV were obtained by the two radiologists. The ICC is widely accepted as follows: below 0.5, poor reliability; between 0.5 and 0.75, moderate reliability; between 0.75 and 0.9, good reliability; and above 0.90, excellent reliability.[26] The mean values of CV reported by the two radiologists were compared among thin-slice 2D FS-PDWIs before and after the adaptation of dDLR and 3D FS-PD MPV images using the Tukey−Kramer honestly significant difference (HSD) test. Statistical significance was inferred for P <0.05.

Evaluations of anatomical structure visualization, image noise, and motion artifacts in thin-slice 2D FS-PDWIs and 3D FS-PD MPV images were analyzed statistically using the Wilcoxon signed-rank test. Statistical significance was inferred for P <0.05.

Inter-rater reliability coefficients between thin-slice 2D FS-PDWIs after dDLR and 3D FS-PD MPV images were analyzed using Gwet's AC_2. Calculation of Gwet's AC_2 was performed with software (R ver. 4.1.0 using irrCAC package ver. 1.0; https://CRAN.R-project.org/package=irrCAC). Agreement was interpreted as follows: less than 0, poor; 0–0.2, slight; 0.21–0.4, fair; 0.41–0.6, moderate; 0.61–0.8, good; and 0.81–1, nearly perfect agreement.[27] In addition, 95% confidence intervals (CIs) were calculated.

Results

Eighteen patients (9 males and 9 females; mean age 64.1 years old, range 21 − 85 years old) who received MRI of the shoulder joint were enrolled. Eighteen shoulders (7 right side and 11 left side) were examined. Table 2 shows the clinical diagnosis of the patients.

Table 2 Clinical diagnosis of the patients

Patient	Clinical diagnosis
1	SSp partial tear (bursal surface), SLAP tear (posterosuperior), tenosynovitis of LHBT
2	SSp tendinosis
3	SSc partial tear, LHBT dislocation
4	SSp partial tear (articular surface)
5	Normal*
6	SLAP tear (anterosuperior), paralabral cyst
7	SSp partial tear (bursal surface), SSc partial tear
8	SSp partial tear (articular surface) and full thickness tear in some areas, SSc partial tear
9	Osteoarthritis, SSc partial tear, posterior labral tear, chondral injury
10	SSp partial tear (bursal surface)
11	SSc partial tear
12	SSp full thickness tear, SLAP tear (anterosuperior)
13	SSp full thickness tear, SSc full thickness tear, ISp full thickness tear
14	SSp full thickness tear, SSc full thickness tear, ISp full thickness tear, LHBT tear
15	Normal*
16	SSp partial tear (bursal surface)
17	SSp partial tear (articular surface), SSc partial tear
18	Normal*

ISp, infraspinatus tendon; LHBT, long head of biceps tendon; SSp, supraspinatus tendon; SLAP, superior labrum from anterior to posterior; SSc, subscapularis tendon;. * "Normal" refers to a case in which the patient had shoulder joint symptoms, and an MRI scan was requested and performed on the assumption that some disease was present, but no abnormality was found on the MRI findings.

As the results of quantitative image evaluation methods, the ICCs of CV measured by the two radiologists ranged from 0.79 to 0.95 for all ROI sizes, which corresponded to good to excellent interobserver reproducibility.[26] Figure 2 presents representative images of oblique coronal thin-slice 2D FS-PDWI before dDLR and oblique coronal thin-slice 2D FS-PDWI after dDLR. The CV of thin-slice 2D FS-PDWI after dDLR was significantly lower than that before dDLR for the humerus, supraspinatus muscle, and labrum: $P < 0.05$, $P < 0.05$, and $P < 0.05$, respectively (Fig. 3). Comparison between the CV of thin-slice 2D FS-PDWIs after dDLR and the CV of 3D FS-PD MPV images indicated the CV of thin-slice 2D FS-PDWIs after dDLR as significantly lower than the CV of 3D FS-PD MPV images with respect to the humerus ($P < 0.05$). For the supraspinatus muscle, no significant difference was found between the CV of thin-slice 2D FS-PDWIs after dDLR and the CV of 3D FS-PD MPV images ($P = 0.27$). The CV of 3D FS-PD MPV images was significantly lower than the CV of thin-slice 2D FS-PDWIs after dDLR in the labrum ($P < 0.05$) (Fig. 3).

Regarding qualitative evaluation findings, both readers rated thin-slice 2D FS-PDWIs as higher than 3D FS-PD MPV images for the SSp, infraspinatus tendon, subscapularis tendon, long head of biceps tendon, cartilage, labrum, and noise ($P < 0.05$), except for artifacts (Figs. 4–7) (Table 3).

Inter-rater reliability coefficients of anatomical structures, noise, and artifacts in thin-slice 2D FS-PDWIs and 3D FS-PD MPV images produced almost-perfect agreement between the two radiologists with Gwet's AC_2 value (Table 4).

Discussion

Scanning thin-slice 2D images has been regarded as difficult because of the decrease of SNR by decreased voxel volume and cross talk artifacts, but the denoising technique by DLR has made it possible.[4,28] The usefulness of applying dDLR to thin-slice 2D images of the knee joint has already been reported. In this report, parallel imaging as acceleration technique was used to obtain thin-slice 2D images.[4] In contrast, in the present study, not only parallel imaging but also

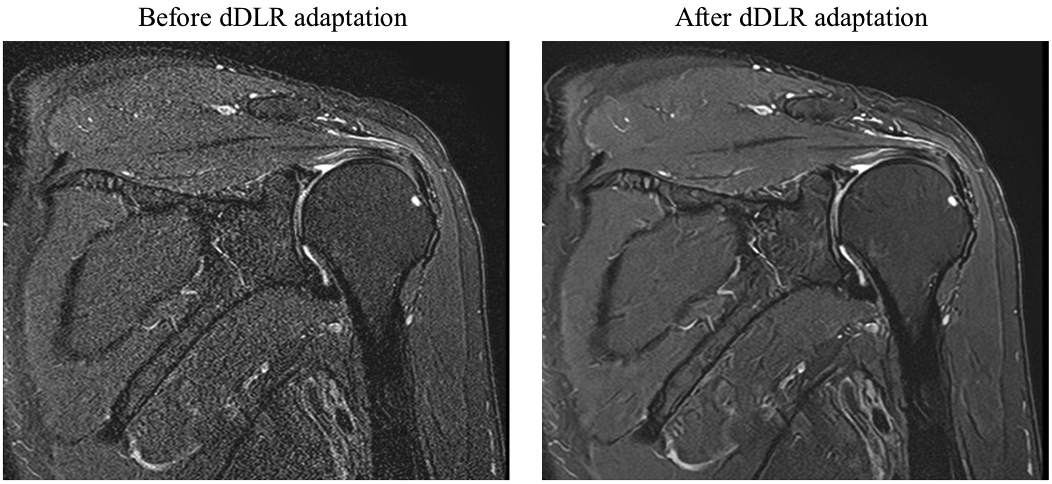

Fig. 2 Denoising effect by dDLR in thin-slice 2D FS-PDWI. The left panel shows a conventional thin-slice 2D FS-PDWI. The right panel shows an image with less noise after applying dDLR to the thin-slice 2D FS-PDWI shown in the left panel. dDLR, denoising approach with deep learning-based reconstruction; 2D FS-PDWI, two-dimensional fat-saturated proton density-weighted image.

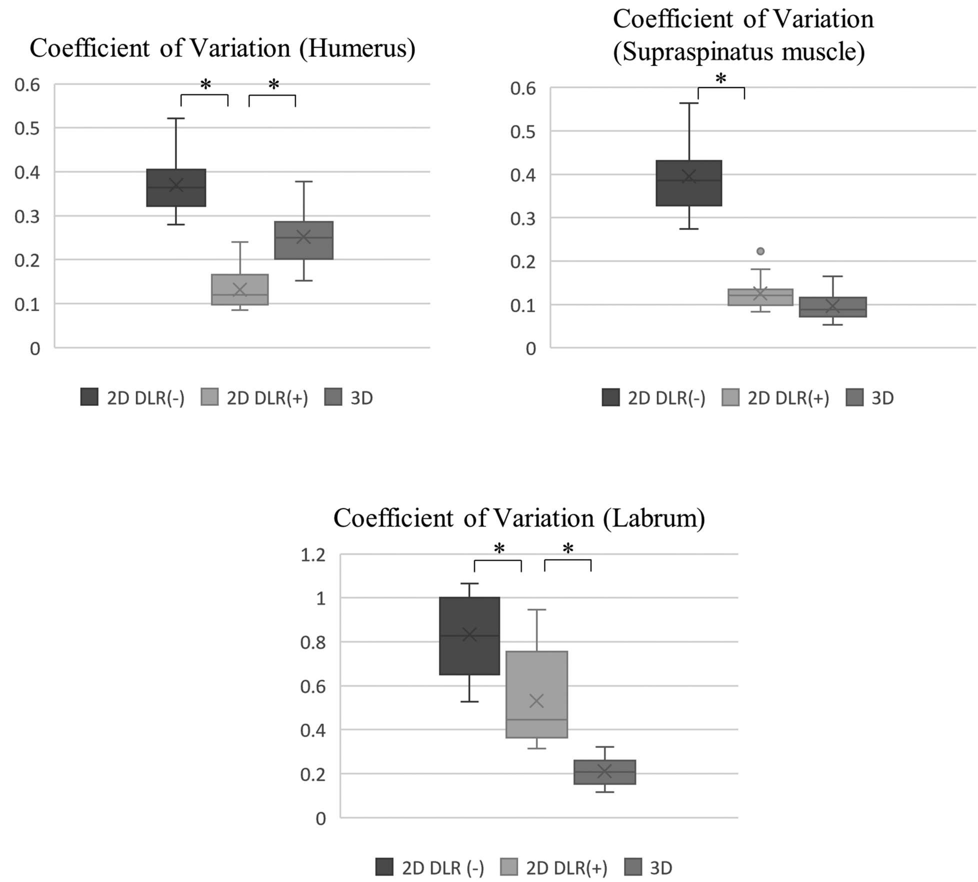

Fig. 3 Results of CV at the humerus, supraspinatus muscle, and labrum among thin-slice 2D FS-PDWIs before and after adaptation of dDLR and 3D FS-PD MPV images. The CV of thin-slice 2D FS-PDWIs after dDLR was significantly lower than that before dDLR for the humerus, supraspinatus muscle, and labrum (*$P < 0.05$, *$P < 0.05$, and *$P < 0.05$, respectively). The CV of thin-slice 2D FS-PDWIs after dDLR was significantly lower than the CV of 3D FS-PD MPV images with respect to the humerus (*$P < 0.05$). For the supraspinatus muscle, no significant difference was found between the CV of thin-slice 2D FS-PDWIs after dDLR and the CV of 3D FS-PD MPV images ($P = 0.27$). The CV of 3D FS-PD MPV images was significantly lower than the CV of thin-slice 2D FS-PDWIs after dDLR in the labrum (*$P < 0.05$). CV, coefficient of variation; 2D FS-PDWIs, two-dimensional fat-saturated proton density-weighted images; dDLR, denoising approach with deep learning-based reconstruction; 3D FS-PD MPV, three-dimensional fat-saturated proton density multi-planar voxel.

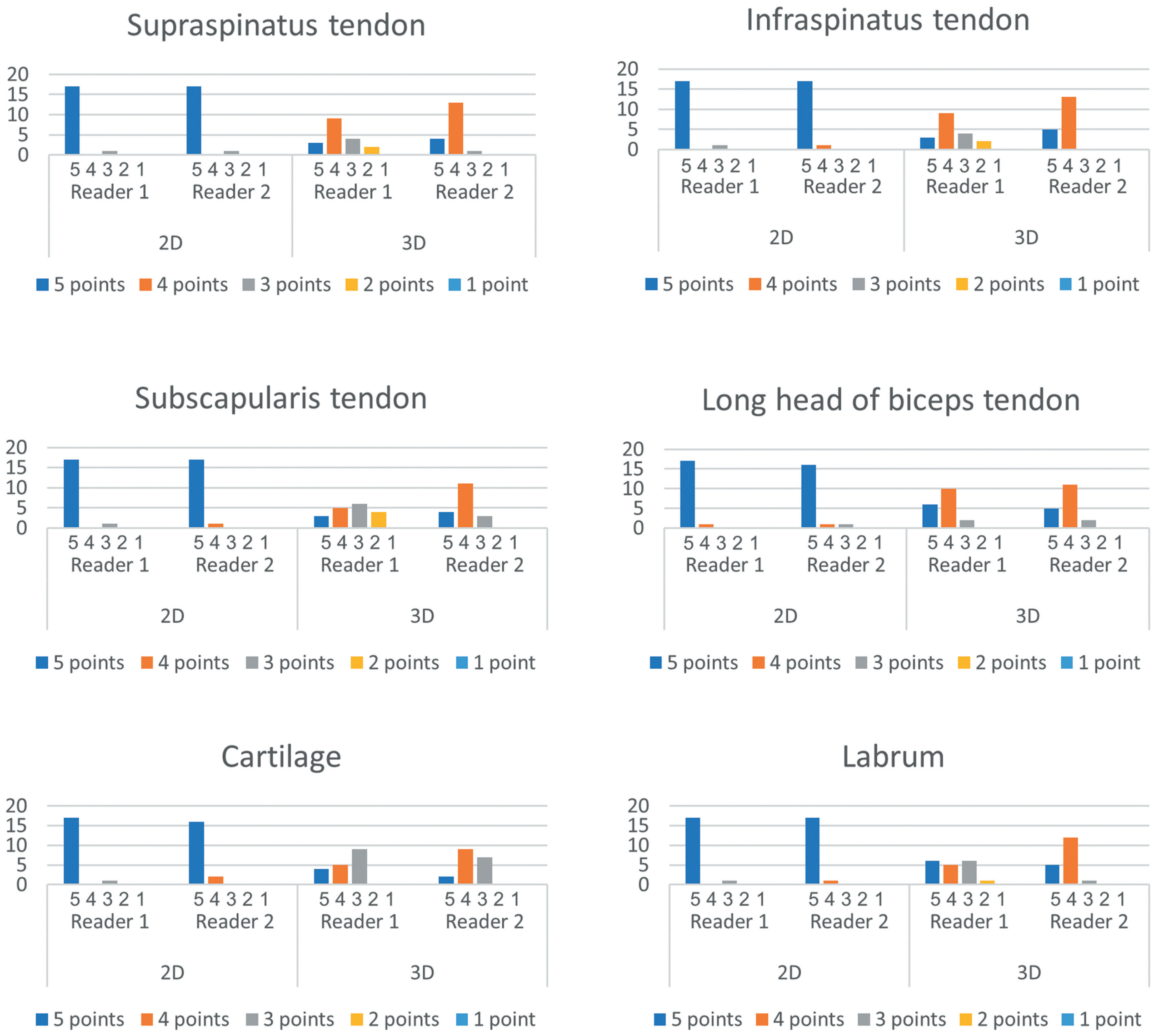

Fig. 4 The score distribution in thin-slice 2D FS-PDWIs and 3D FS-PD MPV images for each anatomical structure. 2D FS-PDWIs, two-dimensional fat-saturated proton density-weighted images; 3D FS-PD MPV, three-dimensional fat-saturated proton density multi-planar voxel.

partial Fourier technique was used. We hypothesized that dDLR would be useful to obtain high-quality thin-slice 2D images of the shoulder joint using both parallel imaging and partial Fourier technique, and we evaluated the following: 1) Denoising effect of dDLR on thin-slice 2D images in comparison to 3D images as quantitative evaluation, 2) visual evaluation of anatomical structures as qualitative evaluation.

For this study, we performed rapid acquisition sequence using both parallel imaging and partial Fourier technique to obtain 2D thin-slice images of three separate imaging planes with acquisition times as close as possible to those used for the 3D scan. The denoising efficiency of dDLR was demonstrated clearly by quantifying the CV of thin-slice 2D FS-PDWIs before and after dDLR. Despite thin-slice and the use of rapid scan techniques such as parallel imaging and partial Fourier technique, dDLR was able to denoise 2D thin-slice images efficiently and to improve SNR. Comparison between thin-slice 2D FS-PDWIs after dDLR and 3D FS-PD MPV images revealed that the qualitative evaluation showed image noise as significantly lower in thin-slice 2D FS-PDWIs. When 2D images were compared with 3D images, thin-slice 2D FS-PDWIs after dDLR showed significantly lower and almost identical CVs of the humerus and SSp, respectively. However, in the labrum, the CV of 3D FS-PD MPV images was significantly lower than that in thin-slice 2D FS-PDWIs after dDLR. Because 2D acquisition has a longer TR than that of 3D, longitudinal magnetization recovers sufficiently even for tissues with

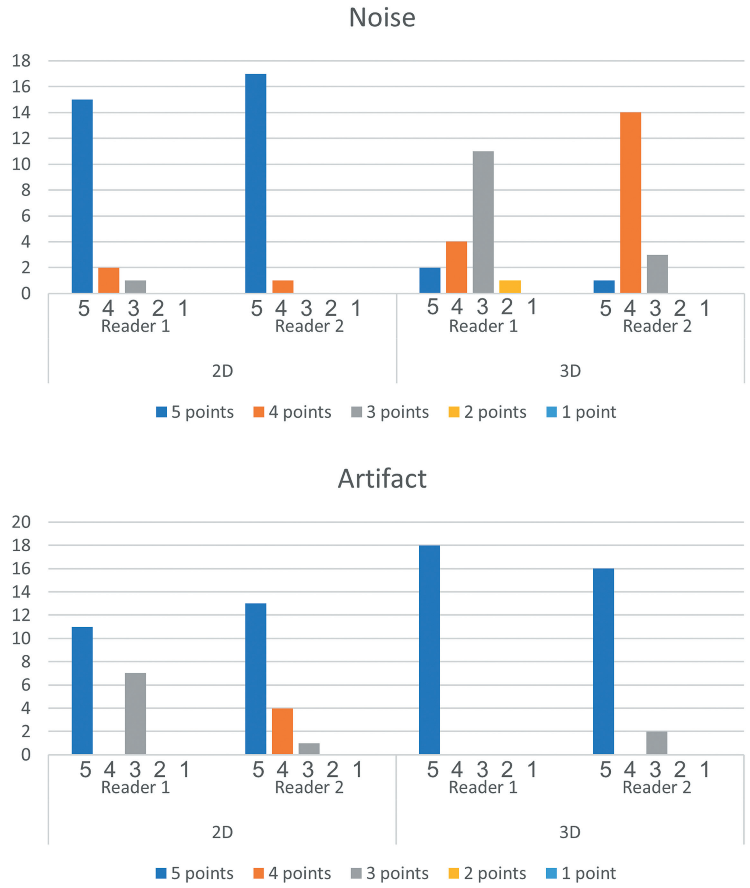

Fig. 5 The score distribution of noise and artifact in thin-slice 2D FS-PDWIs and 3D FS-PD MPV images 2D FS-PDWIs, two-dimensional fat-saturated proton density-weighted images; 3D FS-PD MPV, three-dimensional fat-saturated proton density multi-planar voxel.

longer T1 values such as fibrocartilage tissues; moreover, the signal value increases more for 2D than for 3D.[29,30] In this regard, a lower CV is expected for 2D. However, the 3D acquisition has advantages in terms of the image noise because the number of the slice encodings functions as a signal averaging effect. Moreover, the joint fluid adjacent to labrum was able to increase the mean signal intensity of the labrum, which is a small structure in the joint, because of the signal mixture in the slice encoding direction and image blurring of 3D. When these effects in 3D are dominant in CV measurements, the CV of 3D can be expected to be a lower value. However, thin-slice 2D FS-PDWIs were rated better in the qualitative evaluation. Worse rating in 3D FS-PD MPV images is attributable to blurring and other factors that are unique to 3D images. Therefore, a lower CV does not necessarily mean that anatomical structures are easier to delineate.[10,31]

Regarding qualitative evaluation, both readers rated thin-slice 2D FS-PDWIs after dDLR as better than 3D FS-PD MPV images, with the exception of motion artifacts. The reason the thin-slice 2D FS-PDWIs is evaluated as lower than the 3D FS-PD MPV images in terms of motion artifacts is that the thin-slice 2D FS-PDWI was scanned with a concatenation of two, which results in a marked degree of slice misalignment when motion occurs, even with the rapid acquisition. Motion artifacts of this type would become less conspicuous by setting the concatenation to one.[4] In general, the 3D TSE sequence has a longer scan time than the conventional 2D sequence and is more sensitive to motion,[9] which can degrade the image quality with blurring and ringing. Therefore, scanning the thin-slice 2D FS-PDWIs in each imaging plane separately with a concatenation of one will result in a lower likelihood of motion artifact compared to scanning the 3D FS-PD MPV images.

Regarding inter-rater reliability coefficients, both thin-slice 2D FS-PDWIs and 3D FS-PD MPV images showed almost perfect agreement. Thin-slice 2D FS-PDWIs tended to have a higher Gwet's AC_2 score than 3D FS-PD MPV images. The range of 95% CI was also wider for 3D FS-PD MPV images than for thin-slice 2D FS-PDWIs. These results suggest that thin-slice 2D FS-PDWIs will yield more reproducible findings when interpreting images, which supports the results presented in our earlier report showing higher consistency when diagnosing abnormal findings from knee MRI.[4]

The salient advantages of thin slice 2D images using dDLR are its high in-plane resolution and thin slice

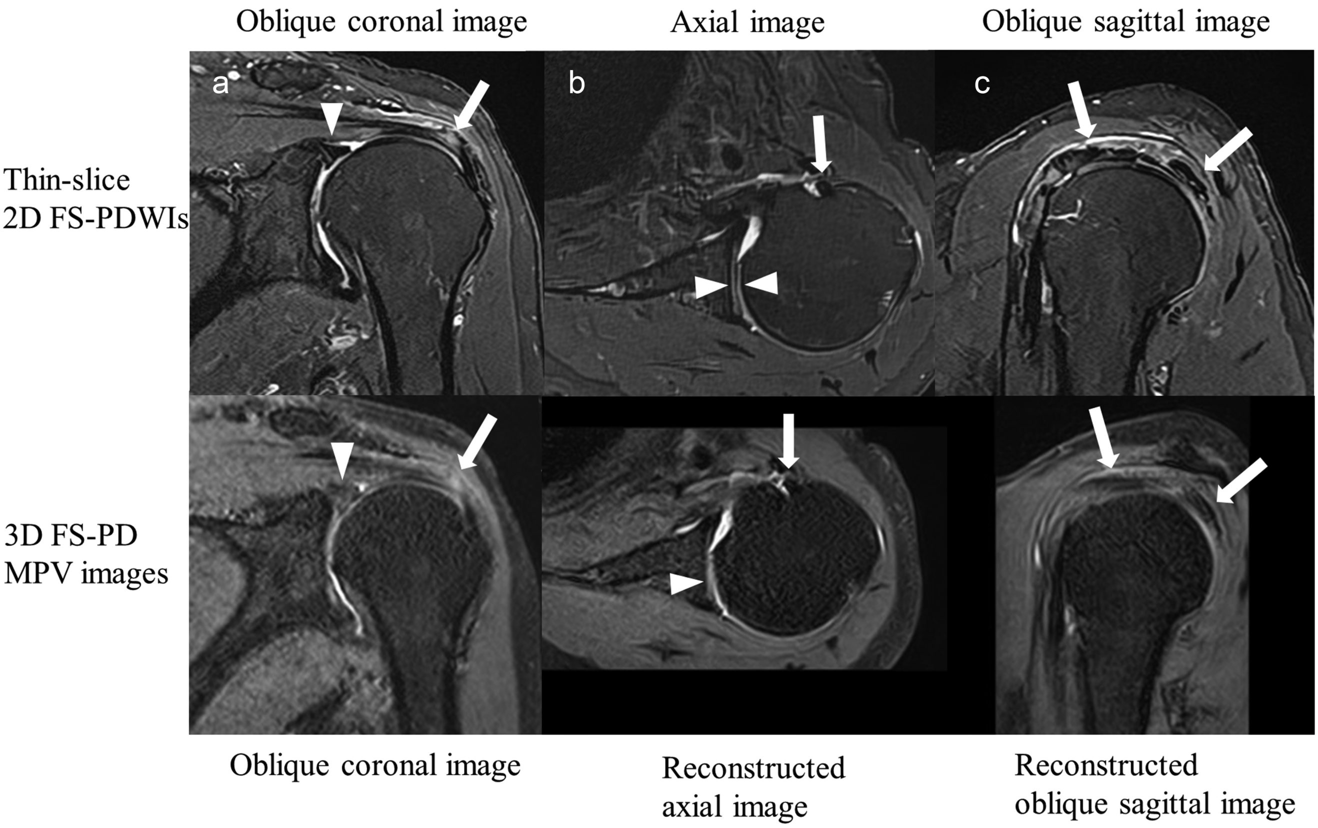

Fig. 6 Comparison between thin-slice 2D FS-PDWIs and 3D FS-PD MPV images for a 78 year-old woman. (**a**), In oblique coronal images, the supraspinatus tendon (arrow) and labrum (arrowhead) in thin-slice 2D FS-PDWI are more clearly visible than in 3D FS-PD MPV image. (**b**) In the axial images, the appearance of long head of biceps tendon (arrow) is not so different between both images. Regarding the cartilage (arrowhead), the thin-slice 2D FS-PDWI clearly depicts the humeral and scapular cartilage, respectively, whereas the 3D FS-PD MPV image shows less clear separation of the cartilage. (**c**), In oblique sagittal images, the supraspinatus and infraspinatus tendons (arrow) in the thin-slice 2D FS-PDWI are much clearer than in the 3D FS-PD MPV image. In the 3D FS-PD MPV image, both tendons appear blurred because of blurring. 2D FS-PDWI, two-dimensional fat-saturated proton density-weighted image; 3D FS-PD MPV, three-dimensional fat-saturated proton density multi-planar voxel.

Table 3 Visual assessment results

Visual assessment	Reader 1				Reader 2			
	2D†		3D¶		2D†		3D¶	
	Mean	SD	Mean	SD	Mean	SD	Mean	SD
SSp*	4.89	0.46	3.72	0.87	4.89	0.46	4.17	0.5
ISp*	4.89	0.46	3.72	0.87	4.94	0.23	4.23	0.45
SSc*	4.89	0.46	3.39	1.01	4.94	0.23	4.06	0.62
LHBT*	4.94	0.23	4.22	0.63	4.83	0.5	4.17	0.6
Cartilage*	4.89	0.46	3.72	0.8	4.89	0.31	3.72	0.65
Labrum*	4.89	0.46	3.89	0.94	4.94	0.23	4.22	0.53
Noise*	4.78	0.53	3.39	0.76	4.94	0.23	3.89	0.46
Artifacts	4.22	0.97	5	0	4.67	0.58	4.78	0.63

Both readers rated thin-slice 2D FS-PDWIs higher than 3D FS-PD MPV images for supraspinatus tendon, infraspinatus tendon, subscapularis tendon, long head of biceps tendon, cartilage, labrum, and noise ($P < 0.05$ and $P < 0.05$, respectively). ISp, infraspinatus tendon; FS-PDWIs, fat-saturated proton density-weighted images; FS-PD MPV, fat-saturated proton density multi-planar voxel; LHBT, long head of biceps tendon; SD, standard deviation; SSp, supraspinatus tendon; SSc, subscapularis tendon; †2D means “thin-slice 2D FS-PDWIs.” ¶3D means “3D FS-PD MPV images.” *Wilcoxon signed-rank test showed $P < 0.05$ for both readers.

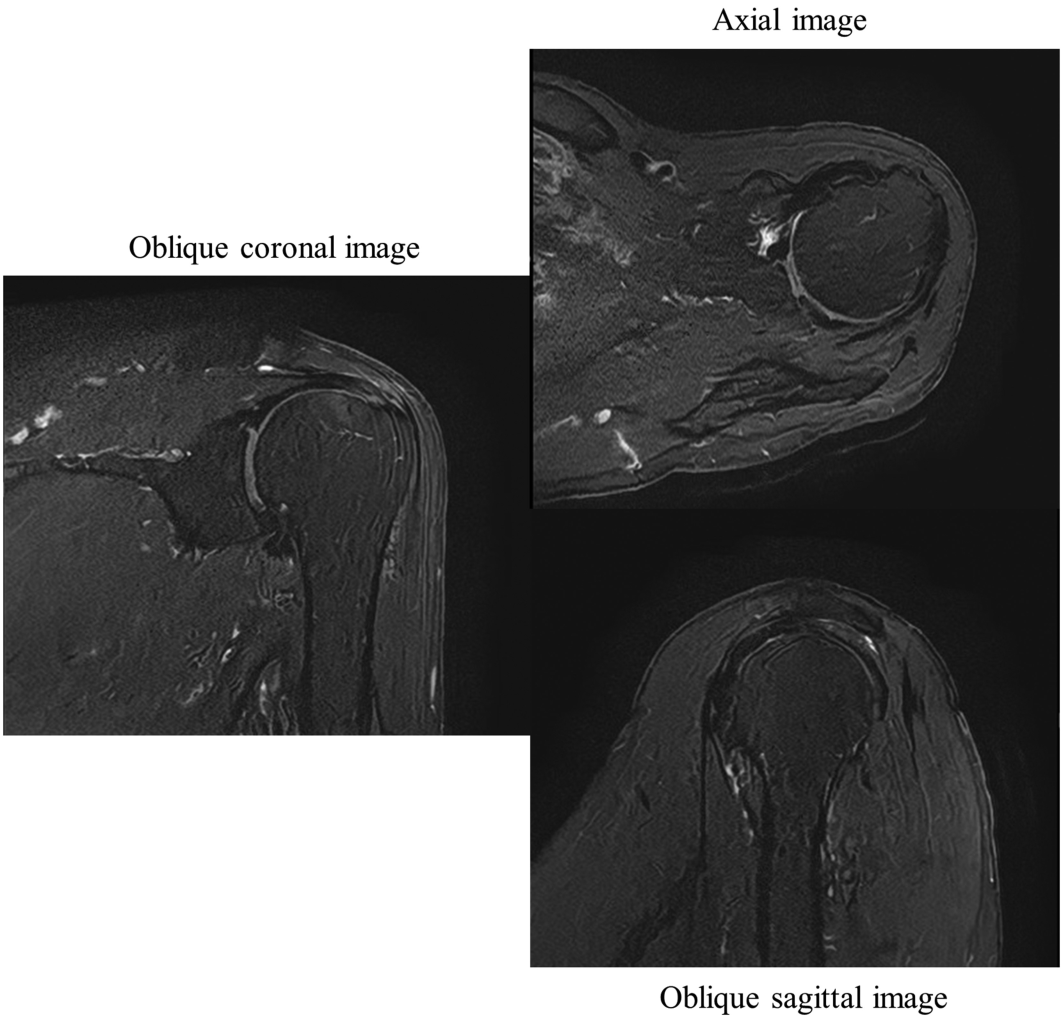

Fig. 7 Motion artifacts in the thin-slice 2D FS-PDWIs. Motion artifacts can be seen in oblique coronal image, axial image, and oblique sagittal image of the same patient. Both radiologists rated the score 3. Although motion artifact was seen, anatomical structures could be evaluated. 2D FS-PDWIs, two-dimensional fat-saturated proton density-weighted images.

Table 4 Results of inter-rater reliability coefficients with Gwet's AC_2

	2D†	95% CI	3D¶	95% CI
SSp	1	1, 1	0.84	0.69, 0.99
ISp	1	0.99, 1	0.84	0.65, 1
SSc	1	0.99, 1	0.76	0.6, 0.93
LHBT	0.99	0.98, 1	0.95	0.91, 0.99
Cartilage	0.99	0.98, 1	0.88	0.81, 0.96
Labrum	1	0.99, 1	0.84	0.73, 0.96
Noise	0.99	0.97, 1	0.88	0.81, 0.96
Artifacts	0.9	0.79, 1	0.97	0.92, 1

Inter-rater reliability coefficients using Gwet's AC_2 for both 2D and 3D showed almost perfect agreement. CI, confidence interval; ISp, infraspinatus tendon; LHBT, long head of biceps tendon; SSp, supraspinatus tendon; SSc, subscapularis tendon. †2D means "thin-slice 2D fat-saturated proton density-weighted images." ¶3D means "3D fat-saturated proton density multi-planar voxel images."

thickness. These minimize the partial volume effect attributable to slice thickness, which has been a difficulty in the past.[6,10,11] In addition, the higher in-plane and higher slice resolution also allow MPR to be created as in 3D images, as reported previously for knee MRI by Kakigi et al.,[4] although three imaging planes were scanned separately for this study. While previous knee joint study aimed to obtain higher resolution images with sufficient acquisition time to create MPR images,[4] this study aimed to obtain high-resolution images in each of three imaging planes with shorter acquisition time by using both parallel imaging and partial Fourier technique. If single-plane thin-slice images alone were sufficient for diagnosing joint disorders, then the acquisition time would be reduced by about one-third.

In the study by Kakigi et al.,[4] lesions were evaluated on thin-slice 2D MRI of the knee joint. They were able to point out lesions with greater confidence and consistency. Although lesions were not evaluated in this study, it is thought that thin-slice 2D MRI can be utilized to clearly delineate lesions in small anatomical structures. We believe that it may be clinically useful in the diagnosis of shoulder joint disease.

This study has several limitations. The study involved only a small number of enrolled patients at a single institution. Future evaluation with a larger number of patients might be necessary. In addition, because the lesions were not evaluated, future studies must correlate the evaluations with surgical findings as gold standards. Moreover, the acquisition time was 8 mins for thin-slice 2D FS-PDWIs and 6 mins 32 sec for 3D FS-PD MPV images. We considered this time to be the limit for scanning a single sequence of 3D FS-PD MPV images. The acquisition time for the thin-slice 2D FS-PDWIs was 8 mins because three imaging planes were scanned, while the acquisition time for the one imaging plane was 2–3 mins. In the future, we would like to evaluate both under the same acquisition time as much as possible. Finally, for quantitative evaluation, we selected the metaphysis of the humerus, the supraspinatus muscle, and the superior portion of the labrum, for which relatively large ROIs could be drawn. Evaluation of SSp, cartilage, and synovial fluids should also have been considered, but we didn't perform these measurements because we couldn't draw ROIs of a sufficient size due to their extreme smallness.

In conclusion, we were able to obtain thin-slice 2D FS-PDWIs with both parallel imaging and partial Fourier technique in oblique coronal, oblique sagittal, and axial planes in a short acquisition time. Thin-slice 2D FS-PDWIs after applying dDLR were demonstrated to be superior to 3D FS-PD MPV images for depicting shoulder joint structures with lower noise. Moreover, thin-slice 2D FS-PDWI findings were highly reproducible, thereby facilitating image evaluation between readers.

Acknowledgments

The authors would like to acknowledge Sadahito Goto, Yoshimitsu Takahashi, Tateo Nakayama, Koji Fujimoto, Makoto Hosono, Yuichi Yamashita, and Nobuyasu Ichinose for their great efforts in developing thin-slice 2D images.

Author Contributions

Conception and design: T.K., R.S.; Acquisition of data: T. K., R.S., R.A., H.N.; Analysis and interpretation of data: T.K., R.S., A.Y.; Patient selection; R.A., S.K., S.M.; Obtaining informed consent: K.K.M., T.S.; Technical assistance in determining optimal imaging sequences and dDLR application: Y.S., R.I. All authors contributed to the drafting of the article or revising it critically for important intellectual content, to the final approval of the version to be published, and agreed to be accountable for all aspects of the work if questions arise related to its accuracy or integrity.

Conflicts of interest

Tsuneo Saga, Kanae Kawai Miyake, and Hitomi Numamoto were endowed chairs of Industry–Academia Collaboration Project between Kyoto University and Canon Medical Systems Corporation. Takahide Kakigi and Ryuzo Arai received more than 50,000 JPY from Canon Medical Systems Corporation annually. Yuichiro Sano and Rimika Imai are employees of Canon Medical Systems Corporation. Other authors declare that they have no conflict of interest.

References

1. Del Grande F, Guggenberger R, Fritz J. Rapid musculoskeletal MRI in 2021: Value and optimized use of widely accessible techniques. *AJR Am J Roentgenol* 2021; 216:704–717.
2. Fritz J, Guggenberger R, Del Grande F. Rapid musculoskeletal MRI in 2021: Clinical application of advanced accelerated techniques. *AJR Am J Roentgenol* 2021; 216:718–733.
3. Del Grande F, Rashidi A, Luna R, et al. Five-minute five-sequence knee MRI using combined simultaneous multi-slice and parallel imaging acceleration: Comparison with 10-minute parallel imaging knee MRI. *Radiology* 2021; 299:635–646.
4. Kakigi T, Sakamoto R, Tagawa H, et al. Diagnostic advantage of thin slice 2D MRI and multiplanar reconstruction of the knee joint using deep learning based denoising approach. *Sci Rep* 2022; 12:10362.
5. Obama Y, Ohno Y, Yamamoto K, et al. MR imaging for shoulder diseases: Effect of compressed sensing and deep learning reconstruction on examination time and imaging quality compared with that of parallel imaging. *Magn Reson Imaging* 2022; 94:56–63.
6. Kloth JK, Winterstein M, Akbar M, et al. Comparison of 3D turbo spin-echo SPACE sequences with conventional 2D MRI sequences to assess the shoulder joint. *Eur J Radiol* 2014; 83:1843–1849.
7. Del Grande F, Delcogliano M, Guglielmi R, et al. Fully automated 10-minute 3D CAIPIRINHA SPACE TSE MRI of the knee in adults: A multicenter, multireader, multifield-strength validation study. *Invest Radiol* 2018; 53:689–697.
8. Fritz J, Fritz B, Thawait GG, Meyer H, Gilson WD, Raithel E. Three-dimensional CAIPIRINHA SPACE TSE for 5-minute high-resolution MRI of the knee. *Invest Radiol* 2016; 51:609–617.
9. Hou B, Li Y, Xiong Y, et al. Comparison of CAIPIRINHA-accelerated 3D fat-saturated-SPACE MRI with 2D MRI sequences for the assessment of shoulder pathology. *Eur Radiol* 2022; 32:593–601.
10. Kijowski R, Gold GE. Routine 3D magnetic resonance imaging of joints. *J Magn Reson Imaging* 2011; 33:758–771.
11. Altahawi FF, Blount KJ, Morley NP, Raithel E, Omar IM. Comparing an accelerated 3D fast spin-echo sequence (CS-SPACE) for knee 3-T magnetic resonance imaging with traditional 3D fast spin-echo (SPACE) and routine 2D sequences. *Skeletal Radiol* 2017; 46:7–15.
12. Feinberg DA, Hale JD, Watts JC, Kaufman L, Mark A. Halving MR imaging time by conjugation: demonstration at 3.5 kG. *Radiology* 1986; 161:527–531.

13. MacFall JR, Pelc NJ, Vavrek RM. Correction of spatially dependent phase shifts for partial Fourier imaging. *Magn Reson Imaging* 1988; 6:143–155.
14. Ueda T, Ohno Y, Yamamoto K, et al. Deep learning reconstruction of diffusion-weighted MRI improves image quality for prostatic imaging. *Radiology* 2022; 303:373–381.
15. Ueda T, Ohno Y, Yamamoto K, et al. Compressed sensing and deep learning reconstruction for women's pelvic MRI denoising: Utility for improving image quality and examination time in routine clinical practice. *Eur J Radiol* 2021; 134:109430.
16. Tanabe M, Higashi M, Yonezawa T, et al. Feasibility of high-resolution magnetic resonance imaging of the liver using deep learning reconstruction based on the deep learning denoising technique. *Magn Reson Imaging* 2021; 80:121–126.
17. Yokota Y, Takeda C, Kidoh M, et al. Effects of deep learning reconstruction technique in high-resolution non-contrast magnetic resonance coronary angiography at a 3-Tesla machine. *Can Assoc Radiol J* 2021; 72:120–127.
18. Naganawa S, Nakamichi R, Ichikawa K, et al. MR imaging of endolymphatic hydrops: Utility of iHYDROPS-Mi2 combined with deep learning reconstruction denoising. *Magn Reson Med Sci* 2021; 20:272–279.
19. Naganawa S, Ito R, Kawai H, et al. MR Imaging of endolymphatic hydrops in five minutes. *Magn Reson Med Sci* 2022; 21:401–405.
20. Taguchi S, Tambo M, Watanabe M, et al. Prospective validation of vesical imaging-reporting and data system using a next-generation magnetic resonance imaging scanner-is denoising deep learning reconstruction useful? *J Urol* 2021; 205:686–692.
21. Yasaka K, Tanishima T, Ohtake Y, et al. Deep learning reconstruction for the evaluation of neuroforaminal stenosis using 1.5T cervical spine MRI: Comparison with 3T MRI without deep learning reconstruction. *Neuroradiology* 2022; 64:2077–2083.
22. Yasaka K, Tanishima T, Ohtake Y, et al. Deep learning reconstruction for 1.5T cervical spine MRI: Effect on interobserver agreement in the evaluation of degenerative changes. *Eur Radiol* 2022; 32:6118–6125.
23. Akai H, Yasaka K, Sugawara H, et al. Commercially available deep-learning-reconstruction of MR imaging of the knee at 1.5T has higher image quality than conventionally-reconstructed imaging at 3T: A normal volunteer study. *Magn Reson Med Sci* 2023; 22:353–360.
24. Akai H, Yasaka K, Sugawara H, et al. Acceleration of knee magnetic resonance imaging using a combination of compressed sensing and commercially available deep learning reconstruction: A preliminary study. *BMC Med Imaging* 2023; 23:5.
25. Kidoh M, Shinoda K, Kitajima M, et al. Deep learning based noise reduction for brain MR imaging: Tests on phantoms and healthy volunteers. *Magn Reson Med Sci* 2020; 19:195–206.
26. Benchoufi M, Matzner-Lober E, Molinari N, Jannot AS, Soyer P. Interobserver agreement issues in radiology. *Diagn Interv Imaging* 2020; 101:639–641.
27. Landis JR, Koch GG. The measurement of observer agreement for categorical data. *Biometrics* 1977; 33:159–174.
28. Simmons A, Tofts PS, Barker GJ, Arridge SR. Sources of intensity nonuniformity in spin echo images at 1.5T. *Magn Reson Med* 1994; 32:121–128.
29. de Bazelaire CM, Duhamel GD, Rofsky NM, Alsop DC. MR imaging relaxation times of abdominal and pelvic tissues measured in vivo at 3.0T: Preliminary results. *Radiology* 2004; 230:652–659.
30. Khodarahmi I, Fritz J. The value of 3 Tesla field strength for musculoskeletal magnetic resonance imaging. *Invest Radiol* 2021; 56:749–763.
31. Subhas N, Kao A, Freire M, Polster JM, Obuchowski NA, Winalski CS. MRI of the knee ligaments and menisci: Comparison of isotropic-resolution 3D and conventional 2D fast spin-echo sequences at 3T. *AJR Am J Roentgenol* 2011; 197:442–450.